iScience

Article
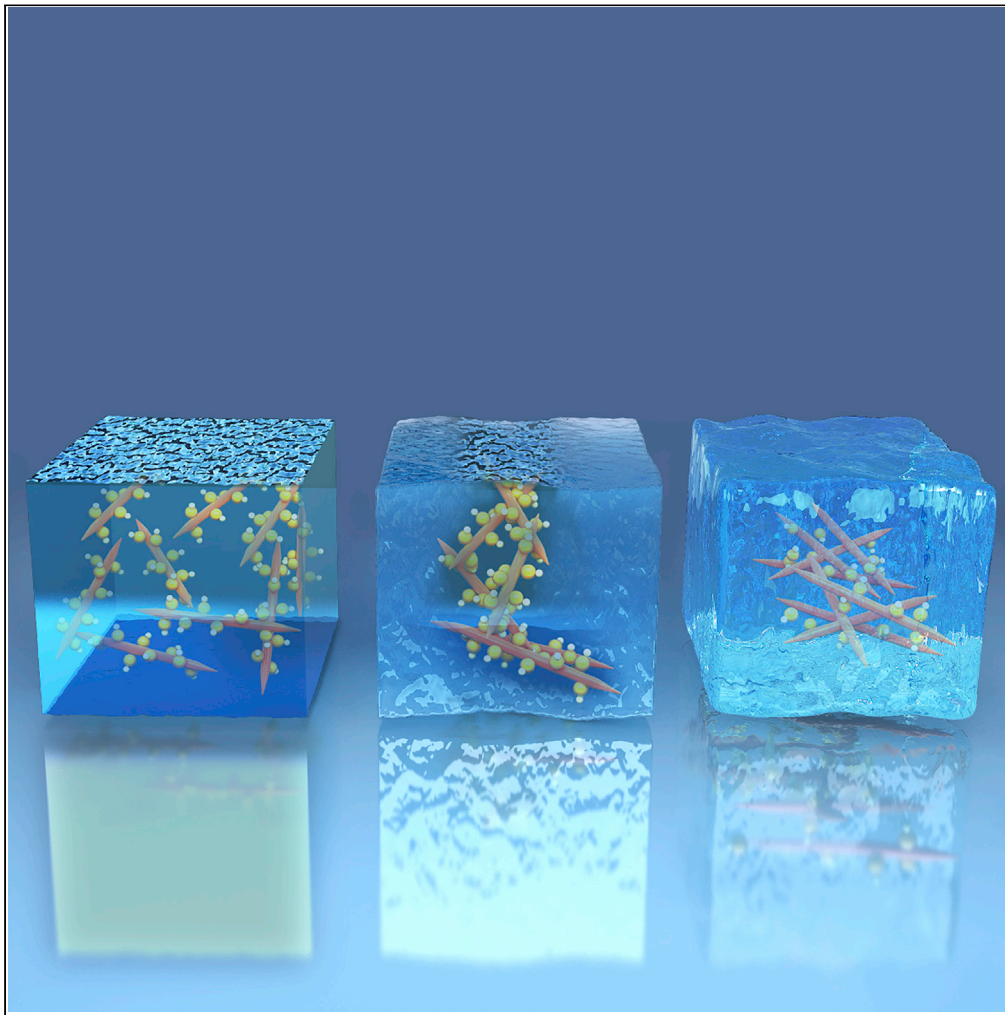
Mechanistic elucidation of freezing-induced surface decomposition of aluminum oxyhydroxide adjuvant

Jiahuan Li, Ge Yu, Zhihui Liang, ..., Xuehu Ma, Changying Xue, Bingbing Sun

bingbingsun@dlut.edu.cn

Highlights

The freezing stress led to the destruction of surface hydroxyl group on AlOOH NPs

Octyl glucoside protected AlOOH NPs from freezing-induced surface decomposition

Octyl glucoside protected vaccines from freezing-induced loss of immunogenicity

Article

Mechanistic elucidation of freezing-induced surface decomposition of aluminum oxyhydroxide adjuvant

Jiahuan Li,[1,2,6] Ge Yu,[1,2,6] Zhihui Liang,[1,2] Min Li,[1,2] Chen Chen,[4] Xin Li,[2] Yiyang Guo,[2] Cheng Yang,[3] Yang Liu,[1,2] Caiqiao Zhang,[5] Weiting Zhang,[5] Jiaxu Liu,[2] Xuehu Ma,[2] Changying Xue,[4] and Bingbing Sun[1,2,7,*]

SUMMARY

The freezing-induced aggregation of aluminum-based (Alum) adjuvants has been considered as the most important cause of reduced vaccine potency. However, the intrinsic properties that determine the functionality of Alum after freezing have not been elucidated. In this study, we used engineered aluminum oxyhydroxide nanoparticles (AlOOH NPs) and demonstrated that cryogenic freezing led to the mechanical pressure-mediated reduction of surface hydroxyl. The sugar-based surfactant, octyl glucoside (OG), was demonstrated to shield AlOOH NPs from the freezing-induced loss of hydroxyl content and the aggregation through the reduction of recrystallization-induced mechanical stress. As a result, the antigenic adsorption property of frozen AlOOH NPs could be effectively protected. When hepatitis B surface antigen (HBsAg) was adjuvanted with OG-protected frozen AlOOH NPs in mice, the loss of immunogenicity was inhibited. These findings provide insights into the freezing-induced surface decomposition of Alum and can be translated to design of protectants to improve the stability of vaccines.

INTRODUCTION

Aluminum-adjuvanted vaccines are temperature-sensitive formulations (Chen et al., 2009; Clausi et al., 2008b; Kurzatkowski et al., 2013, 2018; Milstien et al., 2016). According to the recommendations by World Health Organization (WHO), aluminum-containing vaccines, e.g., diphtheria, hepatitis B, and polio, etc., should be transported and stored within a narrow temperature range at 2–8°C (Organization, 2008, 2015). However, accidental exposures of vaccines below recommended temperatures were frequently reported (Das et al., 2019; Falcon et al., 2020; Maglasang et al., 2018; Murhekar et al., 2013; Organization, 2018; Yauba et al., 2017). A recent review suggested that the risk of exposures to freezing temperature during vaccines transportation and storage was 38% and 33.3% in wealthier countries and 19.3% and 37.1% in lower income countries, respectively (Hanson et al., 2017). Another report highlighted that due to poor refrigeration or the exposure to freezing temperatures, more than $20 million children's vaccines a year were wasted in the US (Kristensen et al., 2011). The annual vaccine wastage caused by accidentally frozen is an obstacle to achieving regional immunization coverage for public health (Organization, 2021).

Freezing of aluminum-adjuvanted vaccines has been demonstrated to lead to compromised immunogenicity. Chen et al. found that the exposure of hepatitis B vaccine to −20°C resulted in a 2.6-fold reduction in antibody titers in serum (Chen et al., 2009). Compared with nonfrozen vaccines, the total anti-HBsAg IgG response was significantly reduced when the HBsAg vaccine containing the frozen aluminum adjuvant was administrated in mice (Clapp et al., 2014). However, it has been demonstrated that the immunogenicity was not affected when vaccines were exposed to freezing temperatures but not frozen (Kartoglu et al., 2010). Mechanistic study has indicated that the low temperature-induced aggregation of the aluminum-salt-based adjuvants is the major cause of reduced immune responses (Clapp et al., 2014; Clausi et al., 2008b; Maa et al., 2003). The mechanical pressure during freezing destroys the lattice structure of the bond between aluminum adjuvant and antigen (Kurzatkowski et al., 2013), thus larger precipitates are formed. By using chemical element determination and thermogravimetry, Kurzatkowski et al. suggested that aluminum hydroxide showed a tendency of water layer destruction in freezing-induced stress, thus causing adhesion and agglomeration between particles, which further affected the binding with antigens

and the immunogenicity (Kurzatkowski et al., 2018). Furthermore, Clausi et al. suggested that the aggregation of aluminum adjuvants was driven by changes in particle surface chemistry and crystallinity mediated by freezing-induced concentrating of salt ions (Clausi et al., 2008b). Existing studies have suggested that the tendency of particles to aggregate could be reduced by using high concentrations of glass-forming excipients (Clausi et al., 2008b). Thus, trehalose and sucrose have been used as protectants in Norovirus and DTaP vaccine formulations, without causing particle aggregation or antigen loss while maintaining the relative potency of the vaccine within acceptable limits (Xu et al., 2021; Xue et al., 2014). However, how freezing changes the intrinsic properties of the aluminum adjuvants remain elusive, which further hinders the design of effective protectants in vaccine formulations.

In this study, we used engineered AlOOH NPs to determine the key physicochemical properties that were compromised during freezing. It was demonstrated that cryogenic freezing could lead to the mechanical-stress-induced destruction of surface hydroxyl contents. With these mechanistic understandings, octyl glucoside was shown to protect aluminum adjuvants from freezing-induced hydroxyl content reduction and the formation of aggregation. By using octyl glucoside, the antigen adsorption properties of aluminum adjuvants could be effectively protected after exposure to freezing temperatures. When formulated in HBsAg vaccine, octyl-glucoside-protected AlOOH NPs exhibited effective adjuvant effects with enhanced total IgG and IgG_1 titers. This study gives insights into the understanding of freezing-induced structural and functional damages of aluminum-based adjuvanted vaccines and further provides design principles for protectants in vaccine formulations.

RESULTS AND DISCUSSION

Physicochemical characterization of AlOOH NPs

AlOOH is the most used adjuvant in human vaccines (Lindblad, 2004; Sun and Xia, 2016). Therefore, engineered AlOOH NPs with well-controlled characteristics were prepared by using hydrothermal method (Liang et al., 2022; Sun et al., 2013). By controlling the synthesis time, the hydroxyl content could be tuned, and these nanorods were named as Rod 1 and Rod 2, respectively. Commercially available Alhydrogel with rod-shaped morphology was used as a control. To determine the effects of freezing on the structure of the adjuvants, $-20°C$ and $-80°C$ were selected as model treatment temperatures. A common model freezing temperature is $-20°C$ (Chen et al., 2009; Clausi et al., 2008b; Kurzatkowski et al., 2013, 2018; Milstien et al., 2016). A temperature of $-80°C$ has been utilized for the storage of certain mRNA vaccines (Mouneer et al., 2021) and was selected in this study to mimic an extreme temperature. Transmission electron microscopy (TEM) was used to characterize the morphology of the materials. For the pristine particles, Rod 1 and Rod 2 exhibited dispersed rod-like shapes. After the adjuvants were exposed to $-20°C$ or $-80°C$, nanorod clusters were formed (Figure 1A). As a control adjuvant, Alhydrogel also showed aggregations after exposure to the freezing temperatures. The aggregations of AlOOH NPs were further confirmed by dynamic light scattering (DLS). Although DLS is not accurate in measuring long-aspect-ratio materials, it can compare agglomeration states of samples (Ji et al., 2012; Wang et al., 2012). After exposure to $-80°C$ for 24 h, the hydrodynamic sizes of Rod 1 and Rod 2 increased from 363 ± 9 nm and 275 ± 5 nm to 609 ± 15 nm and 456 ± 13 nm, respectively. Similarly, when Rod 1 and Rod 2 were exposed to $-20°C$, their hydrodynamic sizes also increased significantly. In addition, when Alhydrogel were exposed to $-20°C$ or $-80°C$, the hydrodynamic sizes increased from 177 ± 1 nm to 3,426 ± 1,295 or 2,212 ± 2,663 nm as well. The particle size distribution of the frozen samples confirmed the formation of larger aggregations (Figures 1B–1D). According to DLVO theory, the stable existence of solutions depends on the potential energy of interaction between particles, and the particles need to overcome a certain energy potential barrier to form aggregation (Piñeres and Barraza, 2011). During the freezing process, the phase change from water to ice increases the volume of the suspension, which could exert enough pressure on the AlOOH nanorods and further drive the particle to overcome the steric repulsion to form particle aggregates (Zapata et al., 1984). In addition, after exposed to $-80°C$ for 24 h, zeta potentials of Rod 1 and Rod 2 decreased from 46 ± 0 mV and 53 ± 2 mV to 30 ± 1 mV and 44 ± 2 mV, respectively. Similarly, when Rod 1 and Rod 2 were exposed to $-20°C$, the zeta potential also decreased. As a control, Alhydrogel also showed a decreased potential from 23 ± 1 mV to 14 ± 0 mV or 15 ± 1 mV (Table 1). The zeta potential of the particles indicated the repulsive force generated by electrostatic interaction between particles. The higher the electrostatic repulsion, the greater the stability of particle suspension. Thus, a reduced or neutral zeta potential could be associated with formation of aggregations (Table 1). The aggregation of particles led to the instability of aluminum adjuvant solutions (Figure S1). Pristine Rod 1 solution (1 mg/mL) was stable within 12 h of
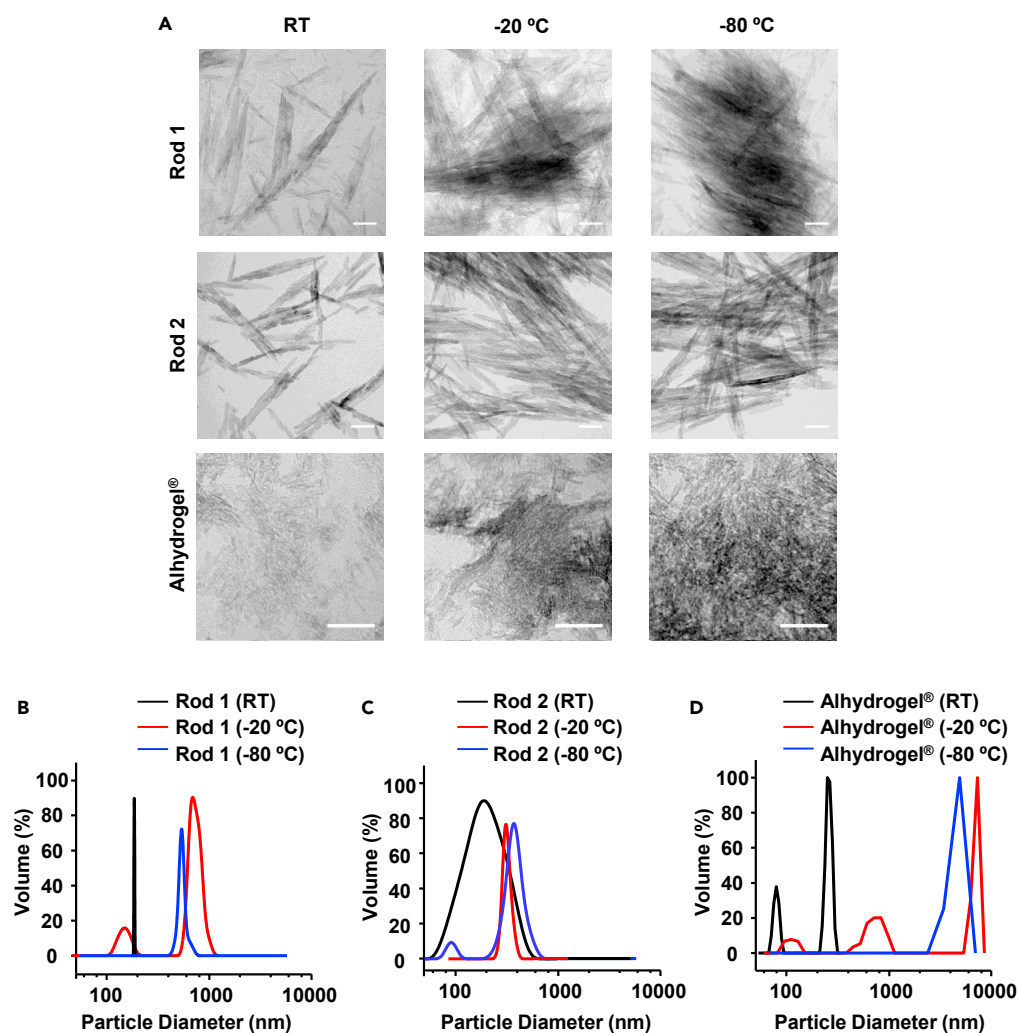
Figure 1. Morphology and size distribution of AlOOH nanorods before and after freezing treatment

(A) Transmission electron microscopy images of AlOOH. AlOOH nanorods were synthesized at 200°C for 2 and 6 h, respectively. Alhydrogel was used as a control. The scale bar is 100 nm.

(B–D) Particle size distribution of (B) Rod 1, (C) Rod 2, and (D) Alhydrogel exposed to RT, −20°C, or −80°C for 24 h.

examination at room temperature (RT). In comparison, significant precipitation was formed within 2 h after exposed to −20°C or −80°C (Figures S1A and S1B).

X-ray diffraction (XRD) patterns suggested that the exposure to freezing temperatures exhibited no significant change in crystal structures of the particles (Figures 2A–2C). However, the mechanical pressure induced by freezing could affect the surface properties of adjuvants. Potentiometric titration was performed to determine the amount of hydroxyl (Al-OH) groups on the particles surface (Meder et al., 2013). After Rod 1 and Rod 2 were exposed to −80°C, the surface hydroxyl contents were significantly reduced from 0.39 ± 0.06 mmol/g and 0.18 ± 0.02 mmol/g to 0.28 ± 0.03 mmol/g and 0.07 ± 0.01 mmol/g, compared with nonfrozen samples (Figure 2D, S2A–S2C, and Table S1). Similarly, when particles were exposed to −20°C, the surface hydroxyl contents also reduced significantly (Figure 2D, S2A–S2C, and Table S1). Furthermore, FTIR analysis of AlOOH NPs was used to validate the titration results. The bands at 1,067 cm^{-1} and 469 cm^{-1} were attributed to symmetric OH deformation (v_s Al-OH) and torsional modes of Al-O (δ Al-O), respectively (Figure 2E), suggesting the loss of hydroxyl groups after exposure to freezing temperatures. The change of the hydroxyl content was determined semi-quantitatively by the area ratio of Al-OH to Al-O peaks. After Rod 1 was exposed to −20°C or −80°C, the content

Table 1. The hydrodynamic sizes, size distributions, and zeta potentials of AlOOH NPs exposed to RT, −20°C, or −80°C for 24 h

Sample ID	Hydrodynamic sizes in water (nm)	Diam.10 (nm)	Diam.50 (nm)	Diam.90 (nm)	Zeta potentials in water (mV)
Rod 1 (RT)	363 ± 9	238	359	540	46 ± 0
Rod 1 (−20°C)	725 ± 23	351	703	1,409	43 ± 1
Rod 1 (−80°C)	609 ± 15	304	608	1,215	30 ± 1
Rod 2 (RT)	275 ± 5	155	269	467	53 ± 2
Rod 2 (−20°C)	440 ± 13	261	455	792	46 ± 1
Rod 2 (−80°C)	456 ± 13	254	467	857	44 ± 2
Alhydrogel® (RT)	177 ± 1	96	176	323	23 ± 1
Alhydrogel® (−20°C)	3,426 ± 1,295	1,371	3,125	7,119	14 ± 0
Alhydrogel® (−80°C)	2,212 ± 2,663	2,172	5,169	12,302	15 ± 1

ratios of Al-OH to Al-O were reduced from 2.04 ± 0.30 to 1.51 ± 0.25 or 1.38 ± 0.31 (Figure 2F). For Alhydrogel, the peak at 1,067 cm^{-1} disappeared (Figure S2D).

Furthermore, thermogravimetric measurement was used to determine the loss of hydroxyl contents on the surface of AlOOH NPs during the freezing. The temperature range between 350°C and 500°C corresponds to the intensive stage of Rod 1 decomposition, which could be attributed to the removal of interstitial water and hydroxyl groups on the AlOOH NPs (Figures S2E and S2G) (Shen et al., 2012). The weight loss of Rod 1 between 350°C and 500°C decreased from 16.13 ± 0.81% to 14.90 ± 0.75% or 13.74 ± 0.69% after exposed to −20°C or −80°C (Table S2). As a control, Alhydrogel also showed a decrease of weight loss between 270°C and 480°C from 16.02 ± 0.80% to 11.89 ± 0.59% or 11.71 ± 0.59% after exposed to −20°C or −80°C for 24 h (Figures S2F, S2H, and Table S2). It can be noted that the hydroxyl loss measured by TGA is not exactly consistent with that measured by surface hydroxyl titration, because both surface hydroxyl groups and the interstitial water could contribute to the weight loss between 350°C and 500°C (Shen et al., 2012). After freezing, only the surface hydroxyl was damaged, thus the reduction of interstitial water measured by TGA could result in a smaller reduction in weight loss. In comparison, the reduction determined by hydroxyl titration was due to the surface hydroxyl loss. Although these two results were not comparable, both are good indication of freezing-induced damages of aluminum-based adjuvant. Collectively, these detailed characterizations confirmed the surface decomposition of AlOOH NP, i.e., the loss of hydroxyl contents. In addition, studies have shown that when the surface hydroxyls on surface of nanomaterials were reduced, the amount of bound water decreased. As a result, the hydration repulsions between nanoparticles were decreased (Ahmed et al., 2011; Tero et al., 2006). According to the extended-DLVO theory, the effect of hydration repulsions on nanoparticle aggregation is more important than electrostatic repulsion. As a result, nanoparticles with smaller hydration repulsions tend to form aggregations (Liu et al., 2015). Therefore, the freezing-induced loss of hydroxyl groups on the surface of AlOOH NPs could also be an important contribution to the agglomeration of nanoparticles.

In order to further elucidate the mechanisms of the loss of surface hydroxyl content, the morphology and size distribution of the ice crystals in the AlOOH NP solution frozen at −80°C were determined (Figures S3A and S3C). TEM, XRD, size distribution, and hydroxyl content analysis confirmed that there was no significant difference in the damages of adjuvants under these two model temperatures (Figures 1 and 2). Thus, the more extreme temperature, i.e., −80°C was selected as the model temperature for further mechanistic studies. It was shown that the freezing led to formation of ice crystals with irregular morphology and larger size distribution (Figure S3A). The uneven distribution of large ice crystals has been shown to lead to compression and mechanical stress to interstitial materials (Amol et al., 2019; Ando et al., 2019; Kurzatkowski et al., 2013; Li et al., 2018; Wang et al., 2018; Xu et al., 2020; Yang et al., 2019, 2020). In addition, it has been suggested that boehmite (γ-AlOOH) could be mechanochemically dehydrated under mechanical pressure, and this transformation was always accompanied by severe microstructure rearrangement (Amol et al., 2019). Thus, the mechanical stress caused by the continuous growth of ice crystals during freezing could contribute to the surface damage of nanoparticles. Meanwhile, the ice water interface has a negative zeta potential, and the surface of AlOOH NPs exhibits a positive charge; thus the electrostatic interaction between the ice crystal surface and the material surface during freezing may be another factor for the loss of hydroxyl content (Castro Neto et al., 2006; Hiroki et al., 1999; Inagawa et al., 2019; Peek et al., 2007).
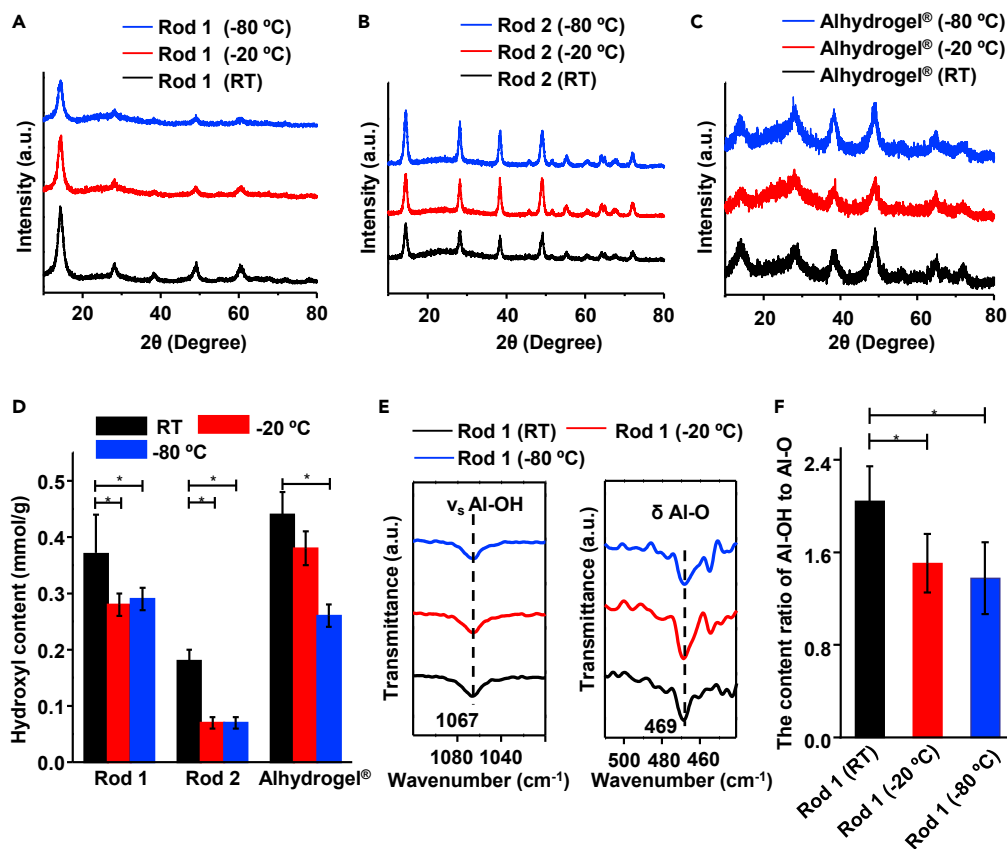
Figure 2. Characterizations of AlOOH NPs before and after freezing temperature exposure

(A–C) XRD patterns of (A) Rod 1, (B) Rod 2, and (C) Alhydrogel exposed to RT, −20°C, or −80°C for 24 h.

(D and E) (D) The hydroxyl content on the surface of AlOOH NPs exposed to RT, −20°C, or −80°C for 24 h (E) FTIR analysis of Rod 1 exposed to RT, −20°C, or −80°C for 24 h.

(F) The content ratio of OH deformation (ν_s Al-OH) and torsional modes of Al-O (δ Al-O). *$p < 0.05$ by Student's t test. N = 3 for each group.

Antigen adsorption on frozen AlOOH NPs

In aluminum-adjuvanted vaccine formulations, antigens are adsorbed to adjuvants to ensure robust immune responses (Shi et al., 2019; Sun et al., 2017). To examine the effect of freezing on antigen adsorption, bovine serum albumin (BSA) was selected as an antigen model to study the adsorption behavior of frozen and nonfrozen adjuvants. According to the above characterization results, −80°C was chosen as the model freezing temperature. With the same concentration of BSA in the solution, the adsorbed BSA contents by frozen adjuvants were significantly lower than that of unfrozen ones (Figures 3A–3C). After exposed to −80°C, the adsorptive capacity reduced from 0.99 and 0.53 mg/mgAl to 0.74 and 0.43 mg/mgAl for Rod 1 and Rod 2, respectively (Table 2). In addition, the adsorptive coefficient decreased from 235.65 and 120.22 mL/mg to 61.72 and 15.85 mL/mg for Rod 1 and Rod 2, respectively. Alhydrogel also showed reduced adsorptive capacity and adsorptive coefficient for BSA after exposed to −80°C. The impact of freezing on adjuvants was further confirmed by adsorption of HBsAg (Figure 3D). For Rod 1, the adsorptive capacity reduced from 0.86 mg/mgAl to 0.70 mg/mgAl, and the adsorptive coefficient decreased from 379 mL/mg to 326 mL/mg after lower temperature treatment at −80°C (Table 2).

The decrease in the adsorptive capacities and adsorptive coefficients of antigens on frozen adjuvants could be attributed to the changes in the physicochemical properties of nanoparticles after freezing. The reduction of the surface charge of the frozen AlOOH nanoparticles directly affected the electrostatic interactions for BSA adsorption, whereas the reduction of surface hydroxyl groups affected the ligand exchange for HBsAg adsorption (Hem and Hogenesch, 2007; Peek et al., 2007). It is worth noting that the reduction of hydroxyl groups on the surface of nanoparticles after freezing was also accompanied by the reduction of
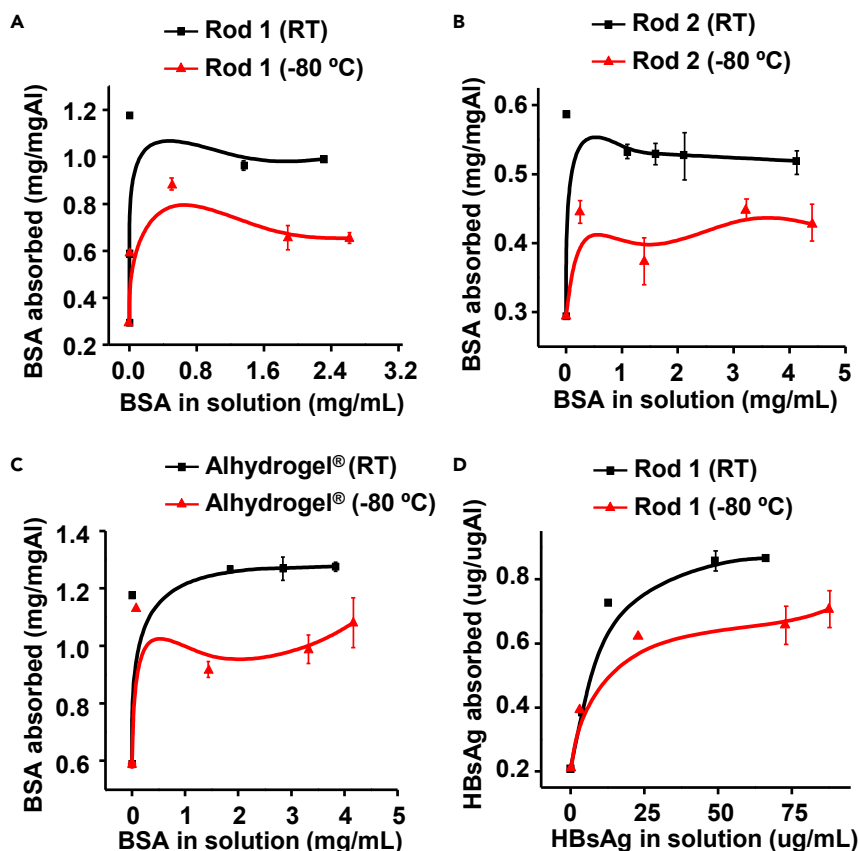
Figure 3. Adsorption behaviors of AlOOH NPs after freezing treatment
(A–C) Adsorption isotherm of BSA by (A) Rod 1, (B) Rod 2, and (C) Alhydrogel exposed to RT or −80°C for 24 h.
(D) Adsorption isotherm of HBsAg by the Rod 1 exposed to RT or −80°C for 24 h.
*p < 0.05 by Student's t test. N = 3 for each group.

the hydration layer, which could lead to reduced hydration repulsion between NPs-NPs and NPs-antigen (Ahmed et al., 2011; Jackman et al., 2015; Park et al., 2021). However, according to the adsorption study (Figure 3), the damage of surface hydroxyl led to reduced adsorptive coefficient, suggesting hydration repulsion did not affect antigen adsorption (Clausi et al., 2008a; Li et al., 2020).

Protective effects of octyl glucoside on the physicochemical properties of AlOOH NPs

Existing study has suggested that freezing changes the elemental composition on the surface of AlOOH particles, mainly in the form of a significant increase in the proportion of Al atoms after freezing due to the damage of the hydration layer (Kurzatkowski et al., 2018). Our mechanistic study has demonstrated that freezing could lead to the loss of hydroxyl content (Figure 2D) and aggregation (Table 1) of AlOOH NPs. Thus, we ask if certain protectant could effectively prevent the loss of functionality of aluminum adjuvants. It has been suggested that the poly hydroxyl head of surfactants could be adsorbed on the nano-particles through hydrogen bonding (Hirsjarvi et al., 2009), and the long alkyl chain tail of surfactants could increase the steric hindrance around the nanoparticles, thus improving the stability of the nanoparticles. The hydrogen bonds between surfactants and materials could also play a protective role on the hydroxyl groups (Hirsjarvi et al., 2009). Therefore, the octyl glucoside with the above-mentioned structures was selected to study its protective effect on adjuvant during freezing. Trehalose, a traditional lyophilized excipient for vaccine, was used as a control. It was shown that in the presence of 0.05% octyl glucoside or 5% trehalose, aggregation was not formed after exposure to −80°C. In addition, DLS measurement indicated that in the presence of 0.05% octyl glucoside, the hydrodynamic size of Rod 1 and Alhydrogel did not increase after freezing, and it remained in the range of 300–400 nm and 400–500 nm (Figures 4B and 4C and Table S3). Furthermore, octyl glucoside effectively protected the surface hydroxyl of Rod 1 during freezing,

Table 2. The adsorptive capacity, coefficient, and monolayer adsorptive capacity of BSA and HBsAg by the AlOOH nanorods exposed to RT or −80°C for 24 h

Antigen	Adjuvant	Adsorptive capacity (mg/mgAl)	Adsorptive coefficient (mL/mg)	Monolayer adsorptive capacity	Coefficient of determination (R^2)
BSA	Rod 1 (RT)	0.99	235.65	0.99	0.99
	Rod 1 (−80°C)	0.74	61.72	0.74	0.99
	Rod 2 (RT)	0.53	120.22	0.53	0.99
	Rod 2 (−80°C)	0.43	15.85	0.43	0.99
	Alhydrogel® (RT)	1.27	117.07	1.27	0.99
	Alhydrogel® (−80°C)	0.99	16.95	1.04	0.99
HBsAg	Rod 1 (RT)	0.86	379	0.88	1.00
	Rod 1 (−80°C)	0.70	326	0.68	1.00

and it remained at 0.34 ± 0.03 mmol/g (Figures 4D, S5A and Table S4). In comparison, 5% trehalose could effectively inhibit the aggregation during the freezing of aluminum adjuvants and maintained the hydrodynamic size in the range of 300–400 nm and 400–500 nm for Rod 1 and Alhydrogel (Figures 4B, 4C, and Table S3). However, trehalose could not inhibit the loss of surface hydroxyl during the freezing process (Figures 4D, S5B, and Table S5), and the surface hydroxyl contents were significantly reduced from 0.34 ± 0.03 mmol/g to 0.26 ± 0.02 mmol/g, compared with nonfrozen samples (Table S5). In addition, the protective effect of sucrose was determined. Similar to trehalose, sucrose inhibited the aggregation of AlOOH NPs when exposed to −80°C (Figure S4). However, it did not protect the loss of surface hydroxyl groups, and the surface hydroxyl group content of sucrose-protected nanoparticles was significantly decreased from 0.29 ± 0.01 mmol/g to 0.23 ± 0.02 mmol/g after freezing (Table S6).

When Rod 1 was exposed to freezing temperature (−80°C) in the presence of 0.05% octyl glucoside, the adsorptive capacity and coefficient of frozen adjuvant to HBsAg were recovered to 1.01 mg/mgAl and 262.08 mL/mg, respectively (Figures 4E and Table 3). However, the presence of 5% trehalose could not effectively protect the decrease of adsorptive capacity and coefficient during the freezing treatment of aluminum adjuvants. Altogether, the effectiveness of octyl glucoside in maintaining the structural stability and adsorptive behavior of AlOOH nanorods during freezing was demonstrated. Its polyhydroxy head could form hydrogen bonds with hydroxyl groups on the surface of AlOOH NPs to protect them from surface damage in the freezing process (Hirsjarvi et al., 2009), and its long hydrophobic carbon chain could exert steric repulsive forces around the particles to avoid aggregation between particles (Figure S6) (Zapata et al., 1984).

Furthermore, it was shown that the recrystallization of ice was inhibited in the presence of octyl glucoside for Rod 1 solution frozen at −80°C (Figure S3B). The morphology and size distribution of ice crystals were more regular and uniform in the presence of octyl glucoside (Figure S3D). Quantitative analysis showed that the average size of ice crystal was decreased from 13.21 ± 4.63 μm to 6.94 ± 1.99 μm. Ice-inhibiting materials, e.g., antifreeze proteins, polyvinyl alcohol, and alginate oligosaccharides, could inhibit the growth and recrystallization of ice crystals by forming hydrogen bonds between hydroxyl groups on the material surface and ice crystals (Jorov et al., 2004; Lee, 2018; Weng et al., 2018; Zhang et al., 2019). Therefore, the polyhydroxy structure of octyl glucoside is conducive to the formation of hydrogen bonds with ice crystals, which could effectively reduce the mechanical pressure to protect the AlOOH NPs.

Protective effects of octyl glucoside on the adjuvanticity of AlOOH NPs

The immunogenicity of vaccines adjuvanted with frozen AlOOH nanorods, and the protective effects of octyl glucoside were assessed *in vivo*. HBsAg was used as a model antigen, and Rod 1 or Alhydrogel was used as adjuvant. The endotoxin levels in Rod 1, Alhydrogel, and octyl glucoside were below 0.5 EU/mL, indicating the absence of endotoxin contamination (Figure S7A). MTS assay eliminated the generation of cytotoxicity by AlOOH NPs and octyl glucoside (Figures S7B and S7C). The mice were vaccinated i.m. on day 0 and 21, and the serum hepatitis-B-specific antibody titers were determined (Figure 5A). HBsAg without adjuvant induced a weak immune response with the total IgG antibody titer at 0.43×10^5 and the IgG_1 antibody titer at 0.18×10^5, respectively. When the antigen was adjuvanted with Rod 1, the total IgG and IgG_1
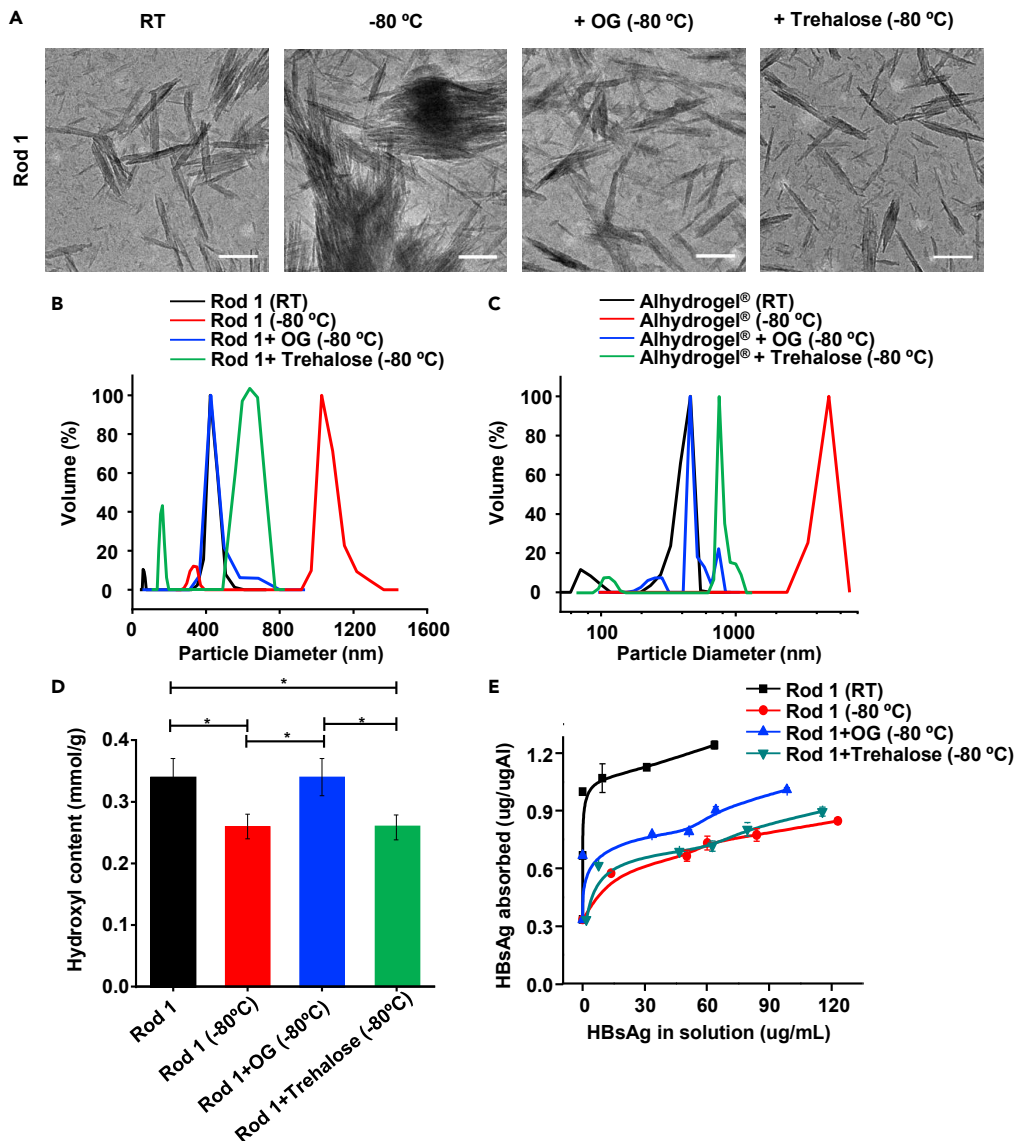
Figure 4. The protective effect of octyl glucoside

(A) Transmission electron microscopy images of Rod 1 exposed to RT or −80°C for 24 h. For the frozen samples, 5% trehalose or 0.05% octyl glucoside was included in the formulation. The scale bar is 300 nm.

(B and C) Particle size distributions for (B) Rod 1 and (C) Alhydrogel after exposed to RT or −80°C for 24 h. For the frozen samples, 5% trehalose or 0.05% octyl glucoside was included in the formulation.

(D) The hydroxyl content on the surface of Rod 1 exposed to RT or −80°C for 24 h. For the frozen samples, 5% trehalose or 0.05% octyl glucoside was included in the formulation.

(E) Adsorption isotherm of HBsAg by Rod 1 exposed to RT or −80°C for 24 h. For the frozen samples, 5% trehalose or 0.05% octyl glucoside was included in the formulation. OG: octyl glucoside. *p < 0.05 by Student's t test. N = 3 for each group.

antibody titers were at 2.17×10^5 and 1.00×10^5, respectively. When the Alhydrogel was used as a control adjuvant, the total IgG and IgG$_1$ antibody titers were at 5.67×10^5 and 2.83×10^5, respectively. However, when HBsAg was adsorbed to the frozen aluminum adjuvants, the humoral immune responses were significantly reduced. The total IgG antibody titers were significantly reduced to 0.85×10^5 and 0.62×10^5 (Figure 5C), and the IgG$_1$ antibody titers were significantly reduced to 0.45×10^5 and 0.11×10^5 when the vaccines were adjuvanted with frozen Rod 1 or Alhydrogel, respectively (Figure 5D). In contrast, when Rod 1 or Alhydrogel were exposed to freezing temperature (−80°C) in the presence of 0.05% octyl glucoside, the total IgG antibody titers of adjuvanted HBsAg vaccine were recovered to 2.00×10^5 and 5.67×10^5

Table 3. The adsorptive capacity, coefficient, and monolayer adsorptive capacity of HBsAg by Rod 1 exposed to RT or −80°C for 24 h

Antigen	Adjuvant	Adsorptive capacity (mg/mgAl)	Adsorptive coefficient (mL/mg)	Monolayer adsorptive capacity	Coefficient of determination (R^2)
HBsAg	Rod 1 (RT)	1.24	1,158.7	1.23	0.99
	Rod 1 (−80°C)	0.85	146.84	0.85	0.98
	Rod 1 + OG (−80°C)	1.01	262.08	0.98	0.98
	Rod 1 + trehalose (−80°C)	0.90	135.13	0.89	0.98

5% trehalose or 0.05% octyl glucoside was included in the formulation. OG: octyl glucoside

and the IgG_1 antibody titers to 1.08×10^5 and 3.19×10^5, respectively (Figures 5C and 5D). Notably, there were wide spread of antibody titers, e.g., the total IgG in Alhydrogel +OG (−80°C) group and the IgG1 in Alhydrogel +OG (−80°C) and Alhydrogel groups. It is possibly due to the variations of animal responses to vaccine formulation (Li et al., 2021; Liang et al., 2022; Tulaeva et al., 2020; Yamayoshi et al., 2021). Nevertheless, statistical analysis confirmed the effectiveness of octyl glucoside in protecting the immune function of the frozen adjuvant (Figures 5C and 5D). The adjuvant effects of octyl glucoside were also determined, and it was shown that it did not induce hepatitis-B-specific antibody responses (Figure S8). It further confirmed that it was octyl-glucoside-protected AlOOH NPs that enhanced the humoral immune responses (Figures 5C and 5D). Moreover, the blood chemistry analysis in adjuvanted mice showed no significant changes in biomarkers for systematic toxicity, suggesting the biocompatibility of the AlOOH NPs and octyl glucoside (Table S7). In addition, we also studied the protective effect of trehalose (Figures 5C and 5D). It was shown that 5% trehalose did exhibit certain protective effect; however, the adjuvanticity was still significantly lower than that of the vaccine prepared with unfrozen adjuvants. According to the above mechanistic study, both octyl glucoside and trehalose exhibited the ability to inhibit the agglomeration of aluminum adjuvant during the freezing (Figures 1B–1D). However, only octyl glucoside could effectively protect the surface hydroxyl groups of aluminum oxyhydroxide adjuvants during the freezing (Figure 4D). Therefore, it suggested that the ability to inhibit both aggregation and the damage of surface hydroxyl by OG could contribute to the protective effect during freezing.

In addition, the protective effect of octyl glucoside on the entire aluminum-adjuvant vaccine formulations during freezing was examined (Figure 5E). When HBsAg was adsorbed to Alhydrogel, the total IgG and IgG_1 antibody titers were at 2.60×10^5 and 1.25×10^5, respectively. However, when the vaccine formulation was exposed to −80°C for 24 h, the humoral immune responses were significantly reduced. The total IgG antibody titers were reduced to 2.66×10^3 (Figure 5F), and the IgG_1 antibody titers were reduced to 1.00×10^3 (Figure 5G). In contrast, when the vaccines were exposed to freezing temperature (−80°C) in the presence of 0.05% octyl glucoside, the total IgG and IgG_1 antibody titers of Alum-adjuvanted HBsAg vaccine were recovered (Figures 5F and 5G). It should be noted that as low as 0.05% octyl glucoside could effectively protect the immunogenic damage caused by freezing in hepatitis B vaccine. The use of minimum amount of protectant could reduce the complexity in vaccine formulations (Drane et al., 2007; Lua et al., 2014). In contrast, 50% PEG 300, 10% propylene glycol, and 50% glycerol have been used as the protectants to maintain and stimulate antibody productions in hepatitis B, DTaP, or DTwP vaccines in mice (Braun et al., 2009; Xue et al., 2014), and 5.55% sucrose has been formulated in lyophilized Norovirus vaccines as the protectant (Xu et al., 2021). All together, these results indicated that octyl glucoside could effectively prevent the freezing-induced compromised immune responses.

Conclusions

In this study, we demonstrated the mechanism of structural and property damage of aluminum adjuvant during the freezing. The freezing leads to aggregation of AlOOH NPs and damage of surface hydroxyl groups due to the mechanical pressure. Based on these mechanistic elucidations, octyl glucoside was demonstrated to effectively inhibit the aggregation and damage of surface properties of adjuvant. Furthermore, it protected the adsorption of antigen and adjuvanticity of AlOOH NPs. This is an innovative adjuvant protectant, and its functionality at lower dosage also minimizes the complexity of the vaccine formulations. In addition, surfactants are commonly used in vaccine formulations to prevent the aggregation and further maintain the stability of antigens. Although the stabilizing effect of octyl glucoside on antigen is not clear, it
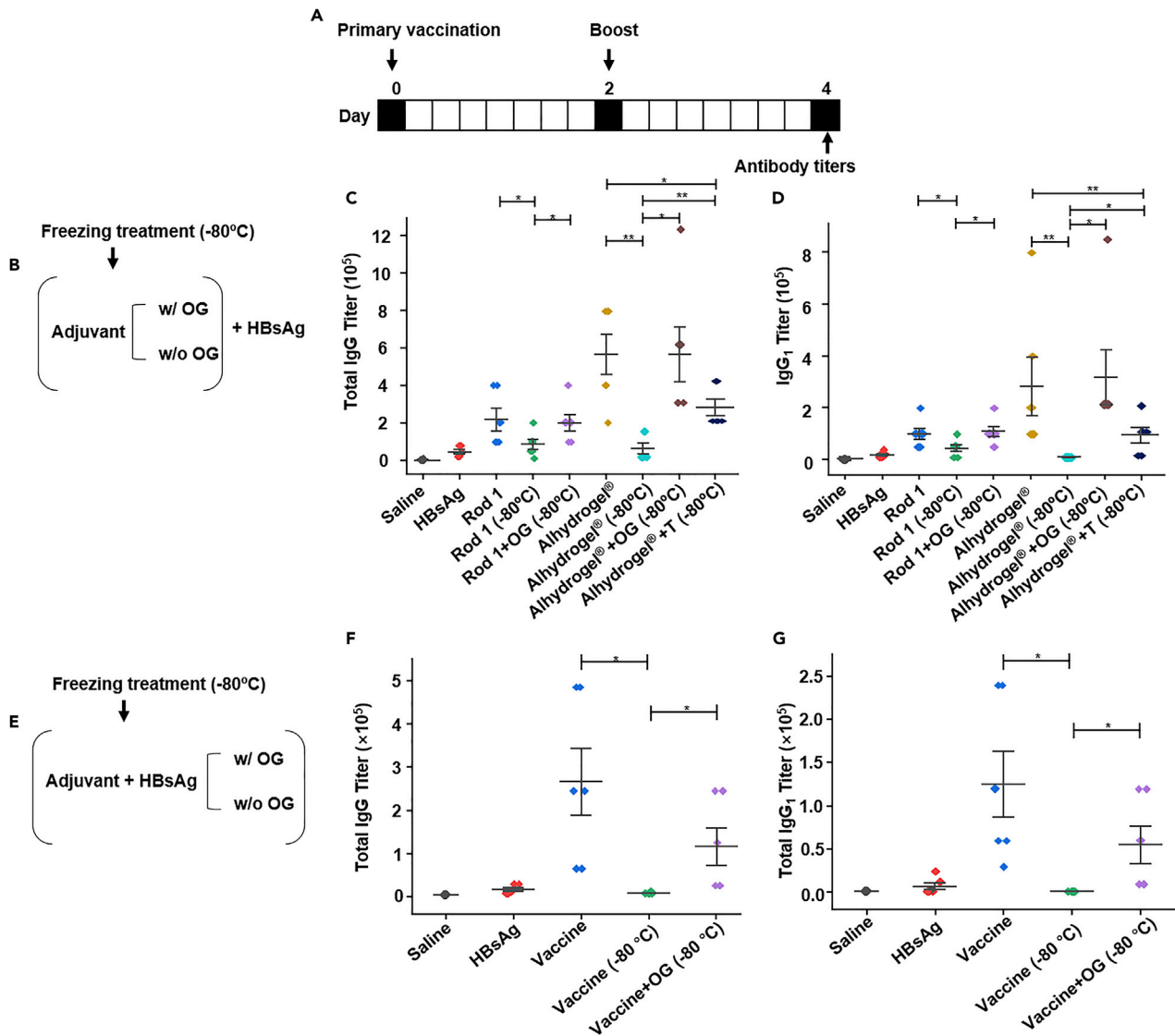
Figure 5. Animal immunization study

(A) Schematic representation of the vaccination procedure. Six-week-old female C57BL/6 mice (n = 6) were vaccinated with HBsAg (2 μg) or HBsAg/Rod1 (2 μg/50 μg Al) through intramuscular administration on day 0, and a boost dose was conducted on day 21. HBsAg/Alhydrogel (2 μg/50 μg Al) was used as control. For the unfrozen samples, Rod 1 or Alhydrogel were kept at RT before binding to HBsAg.

(B) The schematic diagram showing the freezing step: Rod 1 or Alhydrogel were exposed to −80°C before adsorbing to HBsAg. For the frozen adjuvants, 0.05% octyl glucoside or 5% trehalose was included in the formulation.

(C and D) The HBsAg-specific serum (c) total IgG and (D) IgG_1 were determined by ELISA.

(E) The schematic diagram showing the freezing step: HBsAg were adsorbed to Alhydrogel, then the complexes were exposed to −80°C with or without 0.05% octyl glucoside.

(F and G) The HBsAg-specific serum (F) total IgG and (G) IgG_1 were determined by ELISA. OG: octyl glucoside. T: trehalose. *p < 0.05, **p < 0.01 by Student's t test. N = 6 for each group.

is worthy of further detailed formulations studies. These findings can be translated to novel design of protectants for aluminum-adjuvanted vaccines, which is particularly valuable in improving the stability of vaccines exposed to accidental freezing or lyophilized vaccine formulations.

Limitations of the study

In this article, the surface decomposition of the frozen aluminum oxyhydroxide (AlOOH) was demonstrated. Based on detailed mechanistic study, octyl glucoside was shown to inhibit the aggregation and

the surface hydroxyl groups loss of AlOOH adjuvant. Vaccination study showed that octyl glucoside could protect the immune function of the frozen aluminum adjuvants. However, in current study, only HBsAg was used as a model to demonstrate the protective effect of octyl glucoside against freezing damage in vaccine formulation. In future studies, other model antigens, e.g., human papillomavirus (HPV), SARS-CoV-2 spike protein receptor-binding domain (RBD), etc., will be used to examine the efficiency of the protective effect of octyl glucoside against freezing-induced damage.

STAR★METHODS

Detailed methods are provided in the online version of this paper and include the following:

- KEY RESOURCE TABLE
- RESOURCE AVAILABILITY
  - Lead contact
  - Materials availability
  - Data and code availability
- METHOD DETAILS
  - Synthesis and freezing treatment of AlOOH nanorods
  - Physicochemical characterizations
  - Adsorption of antigen
  - Animal vaccination
  - Statistical analysis
- ADDITIONAL RESOURCES

SUPPLEMENTAL INFORMATION

Supplemental information can be found online at https://doi.org/10.1016/j.isci.2022.104456.

AUTHOR CONTRIBUTIONS

J. L and B. S: Conceptualization and Methodology; J. L and B. S: Investigation and Resources; J. L, G. Y, Z. L, M. L, C. C, X. L, Y. G, C. Y, Y. L, C. Z, W. Z, J. L, C. X, and B. S: Experiments and Validation; J. L, B. S, G. Y, and Z. L: Formal Analysis and Data Curation; J. L and G. Y: Writing—Original Draft; J. L, G.Y, M.X, and B. S: Writing—Review & Editing; B. S: Supervision and Funding Acquisition.

DECLARATION OF INTERESTS

The authors declare that they have no known competing financial interests or personal relationships that could have appeared to influence the work reported in this paper.

REFERENCES

Ahmed, S., Madathingal, R.R., Wunder, S.L., Chen, Y., and Bothun, G. (2011). Hydration repulsion effects on the formation of supported lipid bilayers. Soft Matter 7, 1936–1947. https://doi.org/10.1039/c0sm01045f.

Amol, P., Łodziana, Z., Amrute, Z., Schreyer, H., Hannah, S., Weidenthaler, C., Claudia, W., Schüth, F., and Ferdi, S. (2019). High-surface-area corundum by mechanochemically induced phase transformation of boehmite. Science 366, 485–489. https://doi.org/10.1126/science.aaw9377.

Ando, Y., Hagiwara, S., Nabetani, H., Okunishi, T., and Okadome, H. (2019). Impact of ice crystal development on electrical impedance characteristics and mechanical property of green asparagus stems. J. Food Eng. 256, 46–52. https://doi.org/10.1016/j.jfoodeng.2019.03.019.

Braun, L.J., Tyagi, A., Perkins, S., Carpenter, J., Sylvester, D., Guy, M., Kristensen, D., and Chen, D. (2009). Development of a freeze-stable formulation for vaccines containing aluminum salt adjuvants. Vaccine 27, 72–79. https://doi.org/10.1016/j.vaccine.2008.10.027.

Castro Neto, A.H., Pujol, P., and Fradkin, E. (2006). Ice: a strongly correlated proton system. Phys. Rev. B 74, 024302–024312. https://doi.org/10.1103/physrevb.74.024302.

Chang, T., Moses, O.A., Tian, C., Wang, H., Song, L., and Zhao, G. (2021). Synergistic ice inhibition effect enhances rapid freezing cryopreservation with low concentration of cryoprotectants. Adv. Sci. *8*, 2003387–2003400. https://doi.org/10.1002/advs.202003387.

Chen, D., Tyagi, A., Carpenter, J., Perkins, S., Sylvester, D., Guy, M., Kristensen, D.D., and Jones Braun, L. (2009). Characterization of the freeze sensitivity of A hepatitis B vaccine. Hum. Vaccin. *5*, 26–32. https://doi.org/10.4161/hv.5.1.6494.

Clapp, T., Munks, M.W., Trivedi, R., Kompella, U.B., and Braun, L.J. (2014). Freeze-thaw stress of Alhydrogel® alone is sufficient to reduce the immunogenicity of a recombinant hepatitis B vaccine containing native antigen. Vaccine *32*, 3765–3771. https://doi.org/10.1016/j.vaccine.2014.05.037.

Clausi, A., Cummiskey, J., Merkley, S., Carpenter, J.F., Braun, L.J., and Randolph, T.W. (2008a). Influence of particle size and antigen binding on effectiveness of aluminum salt adjuvants in a model lysozyme vaccine. J. Pharm. Sci. *97*, 5252–5262. https://doi.org/10.1002/jps.21390.

Clausi, A.L., Merkley, S.A., Carpenter, J.F., and Randolph, T.W. (2008b). Inhibition of aggregation of aluminum hydroxide adjuvant during freezing and drying. J. Pharm. Sci. *97*, 2049–2061. https://doi.org/10.1002/jps.21143.

Das, M.K., Arora, N.K., Mathew, T., Vyas, B., Sindhu, M., and Yadav, A. (2019). Temperature integrity and exposure to freezing temperature during vaccine transfer under the universal immunization program in three states of India. Indian J. Public Health *63*, 139–142. https://doi.org/10.4103/ijph.ijph_123_18.

Drane, D., Gittleson, C., Boyle, J., and Maraskovsky, E. (2007). ISCOMATRIX adjuvant for prophylactic and therapeutic vaccines. Expert. Rev. Vaccines. *6*, 761–772. https://doi.org/10.1586/14760584.6.5.761.

Falcon, V.C., Porras, Y.V.V., Altamirano, C.M.G., and Kartoglu, U. (2020). A vaccine cold chain temperature monitoring study in the united Mexican states. Vaccine *38*, 5202–5211. https://doi.org/10.1016/j.vaccine.2020.06.014.

Hanson, C.M., George, A.M., Sawadogo, A., and Schreiber, B. (2017). Is freezing in the vaccine cold chain an ongoing issue? a literature review. Vaccine *35*, 2127–2133. https://doi.org/10.1016/j.vaccine.2016.09.070.

Hem, S.L., and Hogenesch, H. (2007). Relationship between physical and chemical properties of aluminum-containing adjuvants and immunopotentiation. Expert. Rev. Vaccines. *6*, 685–698. https://doi.org/10.1586/14760584.6.5.685.

Tamura, H., Tanaka, A., Mita, K.y., and Furuichi, R. (1999). Surface hydroxyl site densities on metal oxides as a measure for the ion-exchange capacity. J. Colloid. Interf. Sci. *209*, 225–231. https://doi.org/10.1006/jcis.1998.5877.

Hirsjarvi, S., Peltonen, L., and Hirvonen, J. (2009). Effect of sugars, surfactant, and tangential flow filtration on the freeze-drying of poly(Lactic Acid) nanoparticles. AAPS PharmSciTech *10*, 488–494. https://doi.org/10.1208/s12249-009-9236-z.

Inagawa, A., Harada, M., and Okada, T. (2019). Charging of the ice/solution interface by deprotonation of dangling bonds, ion adsorption, and ion uptake in an ice crystal as revealed by zeta potential determination. J. Phys. Chem. C. *123*, 6062–6069. https://doi.org/10.1021/acs.jpcc.8b12435.

Jackman, J.A., Tabaei, S.R., Zhao, Z., Yorulmaz, S., and Cho, N.J. (2015). Self-assembly formation of lipid bilayer coatings on bare aluminum oxide: overcoming the force of interfacial water. ACS. Appl. Mater. Interfaces. *7*, 959–968. https://doi.org/10.1021/am507651h.

Ji, Z., Wang, X., Zhang, H., Lin, S., Meng, H., Sun, B., George, S., Xia, T., Nel, A.E., and Zink, J.I. (2012). Designed synthesis of CeO2 nanorods andNanowires for StudyingToxicological effects of high aspect ratio nanomaterials. ACS Nano *6*, 5366–5380. https://doi.org/10.1021/nn3012114.

Jorov, A., Zhorov, B.S., and Yang, D.S. (2004). Theoretical study of interaction of winter flounder antifreeze protein with ice. Protein. Sci. *13*, 1524–1537. https://doi.org/10.1110/ps.04641104.

Kartoglu, U., Ozguler, N.K., Wolfson, L.J., and Kurzatkowski, W. (2010). Validation of the shake test for detecting freeze damage to adsorbed vaccines. Bull. World Health Organ. *88*, 624–631. https://doi.org/10.2471/blt.09.056879.

Kristensen, D., Chen, D., and Cummings, R. (2011). Vaccine stabilization: Research, commercialization, and potential impact. Vaccine *29*, 7122–7124. https://doi.org/10.1016/j.vaccine.2011.05.070.

Kurzatkowski, W., Kartoglu, U., Gorska, P., Glowka, M., Woznica, K., Zasada, A.A., Szczepanska, G., Trykowski, G., Gniadek, M., and Donten, M. (2018). Physical and chemical changes in Alhydrogel damaged by freezing. Vaccine *36*, 6902–6910. https://doi.org/10.1016/j.vaccine.2018.10.023.

Kurzatkowski, W., Kartoglu, U., Staniszewska, M., Gorska, P., Krause, A., and Wysocki, M.J. (2013). Structural damages in adsorbed vaccines affected by freezing. Biologicals *41*, 71–76. https://doi.org/10.1016/j.biologicals.2011.10.011.

Lee, H. (2018). Structures, dynamics, and hydrogen-bond interactions of antifreeze proteins in TIP4P/ice water and their dependence on force fields. PLoS One *13*, 0198887. https://doi.org/10.1371/journal.pone.0198887.

Li, D., Zhu, Z., and Sun, D.-W. (2018). Effects of freezing on cell structure of fresh cellular food materials: a review. Trends Food Sci. Tech. *75*, 46–55. https://doi.org/10.1016/j.tifs.2018.02.019.

Li, K., Dong, F., Gao, F., Bian, L., Sun, S., Du, R., Hu, Y., Mao, Q., Zheng, H., Wu, X., and Liang, Z. (2020). Effect of freezing on recombinant hepatitis E vaccine. Hum. Vaccin. Immunother. *16*, 1545–1553. https://doi.org/10.1080/21645515.2019.1694327.

Li, L., Tan, C., Zeng, J., Luo, C., Hu, S., Peng, Y., Li, W., Xie, Z., Ling, Y., Zhang, X., et al. (2021). Analysis of viral load in different specimen types and serum antibody levels of COVID-19 patients. J. Transl. Med. *19*, 30–38. https://doi.org/10.1186/s12967-020-02693-2.

Liang, Z., Wang, X., Yu, G., Li, M., Shi, S., Bao, H., Chen, C., Fu, D., Ma, W., Xue, C., and Sun, B. (2022). Mechanistic understanding of the aspect ratio-dependent adjuvanticity of engineered aluminum oxyhydroxide nanorods in prophylactic vaccines. Nano. Today. *43*, 101445. https://doi.org/10.1016/j.nantod.2022.101445.

Liang, Z., Yang, Y., Yu, G., Zhu, H., Xia, X., Chen, C., Fu, D., Li, M., Cheng, G., Xue, C., et al. (2021). Engineering aluminum hydroxyphosphate nanoparticles with well-controlled surface property to enhance humoral immune responses as vaccine adjuvants. Biomaterials *275*, 120960. https://doi.org/10.1016/j.biomaterials.2021.120960.

Lindblad, E.B. (2004). Aluminium adjuvants-in retrospect and prospect. Vaccine *22*, 3658–3668. https://doi.org/10.1016/j.vaccine.2004.03.032.

Liu, H.H., Lanphere, J., Walker, S., and Cohen, Y. (2015). Effect of hydration repulsion on nanoparticle agglomeration evaluated via a constant number Monte–Carlo simulation. Nanotechnology *26*, 045708. https://doi.org/10.1088/0957-4484/26/4/045708.

Lua, L.H., Connors, N.K., Sainsbury, F., Chuan, Y.P., Wibowo, N., and Middelberg, A.P. (2014). Bioengineering virus-like particles as vaccines. Biotechnol. Bioeng. *111*, 425–440. https://doi.org/10.1002/bit.25159.

Maa, Y.-F., Zhao, L., Payne, L.G., and Chen, D. (2003). Stabilization of alum-adjuvanted vaccine dry powder formulations: mechanism and application. J. Pharmaceut. Sci. *92*, 319–332. https://doi.org/10.1002/jps.10294.

Maglasang, P.L., Butalid, M.L., Pastoril, M.F., Pratama, A.N., and Tan, E.Y. (2018). A cross-sectional survey on cold chain management of vaccines in cebu, Philippines. Pharm. Pract. *16*, 1167. https://doi.org/10.18549/pharmpract.2018.02.1167.

Meder, F., Kaur, S., Treccani, L., and Rezwan, K. (2013). Controlling mixed-protein adsorption layers on colloidal alumina particles by tailoring carboxyl and hydroxyl surface group densities. Langmuir *29*, 12502–12510. https://doi.org/10.1021/la402093j.

Milstien, J., Kartoglu, U., and Zaffran, M. (2016). Temperature Sensitivity of Vaccines (World Health Organization). [WHO/IVB/06.10].

Mouneer, T.A., Elshaer, A.M., and Aly, M.H. (2021). Novel cascade refrigeration cycle for cold supply chain of COVID-19 vaccines at ultra-low temperature -80°C using ethane (R170) based hydrocarbon pair. World J. Eng. Technol. *09*, 309–336.

Murhekar, M.V., Dutta, S., Kapoor, A.N., Bitragunta, S., Dodum, R., Ghosh, P., Swamy, K.K., Mukhopadhyay, K., Ningombam, S., Parmar, K., et al. (2013). Frequent exposure to suboptimal temperatures in vaccine cold-chain system in India: results of temperature monitoring in 10 states. Bull. World. Health. Organ. *91*, 906–913. https://doi.org/10.2471/blt.13.119974.

Organization, W.H. (2008). Module 1: Cold Chain, Vaccines and Safe-Injection Equipment Management. Training for Mid-level Managers (MLM). *WHO/IVB/08.01*.

Organization, W.H. (2015). How to monitor temepatures in the vaccine supply chain. In WHO Vaccine Management Handbook Module VMH-E2. WHO/IVB/15.04.

Organization, W.H. (2018). Temperature Monitoring Study: A Fully Documented Process to Detect Weaknesses in the Supply Chain (World Health Organization). WHO/IVB/18.04.

Organization, W.H. (2021). Global Health Observatory Data: Immunization Coverage (World Health Organization).

Park, H., Ma, G.J., Yoon, B.K., Cho, N.J., and Jackman, J.A. (2021). Comparing protein adsorption onto alumina and silica nanomaterial surfaces: clues for vaccine adjuvant development. Langmuir 37, 1306–1314. https://doi.org/10.1021/acs.langmuir.0c03396.

Peek, L.J., Martin, T.T., Elk Nation, C., Pegram, S.A., and Middaugh, C.R. (2007). Effects of stabilizers on the destabilization of proteins upon adsorption to aluminum salt adjuvants. J. Pharm. Sci. 96, 547–557. https://doi.org/10.1002/jps.20762.

Piñeres, J., and Barraza, J. (2011). Energy barrier of aggregates coal particle–bubble through the extended DLVO theory. Int. J. Miner. Process. 100, 14–20. https://doi.org/10.1016/j.minpro.2011.04.007.

Shen, S., Ng, W.K., Chia, L.S.O., Dong, Y., and Tan, R.B.H. (2012). Morphology controllable synthesis of nanostructured boehmite and γ-alumina by facile dry gel conversion. Cryst. Growth Des. 12, 4987–4994. https://doi.org/10.1021/cg300915p.

Shi, S., Zhu, H., Xia, X., Liang, Z., Ma, X., and Sun, B. (2019). Vaccine adjuvants: understanding the structure and mechanism of adjuvanticity. Vaccine 37, 3167–3178. https://doi.org/10.1016/j.vaccine.2019.04.055.

Sun, B., Ji, Z., Liao, Y.P., Wang, M., Wang, X., Dong, J., Chang, C.H., Li, R., Zhang, H., Nel, A.E., and Xia, T. (2013). Engineering an effective immune adjuvant by designed control of Shape and crystallinity of aluminum oxyhydroxide nanoparticles. ACS. Nano. 7, 10834–10849. https://doi.org/10.1021/nn404211j.

Sun, B., Ji, Z., Liao, Y.P., Chang, C.H., Wang, X., Ku, J., Xue, C., Mirshafiee, V., and Xia, T. (2017). Enhanced immune adjuvant activity of aluminum oxyhydroxide nanorods through cationic surface functionalization. ACS Appl. Mater. Interfaces 9, 21697–21705. https://doi.org/10.1021/acsami.7b05817.

Sun, B., and Xia, T. (2016). Nanomaterial-based vaccine adjuvants. J. Mater. Chem. B 4, 5496–5509. https://doi.org/10.1039/c6tb01131d.

Tero, R., Watanabe, H., and Urisu, T. (2006). Supported phospholipid bilayer formation on hydrophilicity-controlled silicon dioxide surfaces. Phys. Chem. Chem. Phys. 8, 3885–3894. https://doi.org/10.1039/b606052h.

Tulaeva, I., Cornelius, C., Zieglmayer, P., Zieglmayer, R., Schmutz, R., Lemell, P., Weber, M., Focke-Tejkl, M., Karaulov, A., Henning, R., and Valenta, R. (2020). Quantification, epitope mapping and genotype cross-reactivity of hepatitis B preS-specific antibodies in subjects vaccinated with different dosage regimens of BM32. EBioMedicine 59, 102953. https://doi.org/10.1016/j.ebiom.2020.102953.

Wang, X., Xia, T., Duch, M.C., Ji, Z., Zhang, H., Li, R., Sun, B., Lin, S., Meng, H., Liao, Y.P., et al. (2012). Pluronic F108 coating decreases the lung fibrosis potential of multiwall carbon nanotubes by reducing lysosomal injury. Nano. Lett. 12, 3050–3061. https://doi.org/10.1021/nl300895y.

Wang, Y., Miyazaki, R., Saitou, S., Hirasaka, K., Takeshita, S., Tachibana, K., and Taniyama, S. (2018). The effect of ice crystals formations on the flesh quality of frozen horse mackerel (Trachurus japonicus). J. Texture Stud. 49, 485–491. https://doi.org/10.1111/jtxs.12310.

Weng, L., Stott, S.L., and Toner, M. (2018). Molecular dynamics at the interface between ice and poly(vinyl alcohol) and ice recrystallization inhibition. Langmuir 34, 5116–5123. https://doi.org/10.1021/acs.langmuir.7b03243.

Wharton, D.A., Wilson, P.W., Mutch, J.S., Marshall, C.J., and Lim, M. (2007). Recrystallization inhibition assessed by splat cooling and optical recrystallometry. CryoLetter 28, 61–68.

Xu, C.-C., Liu, D.-K., Guo, C.-X., and Wu, Y.-q. (2020). Effect of cooling rate and super-chilling temperature on ice crystal characteristic, cell structure, and physicochemical quality of super-chilled fresh-cut celery. Int. J. Refrig. 113, 249–255. https://doi.org/10.1016/j.ijrefrig.2020.01.024.

Xu, H., Bhowmik, T., Gong, K., Huynh, T.N.A., Williams, R.O., and Cui, Z. (2021). Thin-film freeze-drying of a bivalent Norovirus vaccine while maintaining the potency of both antigens. Int. J. Pharm. 609, 121126. https://doi.org/10.1016/j.ijpharm.2021.121126.

Xue, H., Yang, B., Kristensen, D.D., and Chen, D. (2014). A freeze-stable formulation for DTwP and DTaP vaccines. Hum. Vaccin. Immunother. 10, 3607–3610. https://doi.org/10.4161/21645515.2014.980195.

Yamayoshi, S., Yasuhara, A., Ito, M., Akasaka, O., Nakamura, M., Nakachi, I., Koga, M., Mitamura, K., Yagi, K., Maeda, K., et al. (2021). Antibody titers against SARS-CoV-2 decline, but do not disappear for several months. EClinicalMedicine 32, 100734. https://doi.org/10.1016/j.eclinm.2021.100734.

Yang, F., Jing, D., Diao, Y., Yu, D., Gao, P., Xia, W., Jiang, Q., Xu, Y., Yu, P., and Zhan, X. (2020). Effect of immersion freezing with edible solution on freezing efficiency and physical properties of obscure pufferfish (Takifugu obscurus) fillets. LWT 118, 108762. https://doi.org/10.1016/j.lwt.2019.108762.

Yang, F., Jing, D., Yu, D., Xia, W., Jiang, Q., Xu, Y., and Yu, P. (2019). Differential roles of ice crystal, endogenous proteolytic activities and oxidation in softening of obscure pufferfish (Takifugu obscurus) fillets during frozen storage. Food Chem. 278, 452–459. https://doi.org/10.1016/j.foodchem.2018.11.084.

Yauba, S., Joelle, S., Jude, N., Tracy, B.O., Marie, K., Charles, N., Hermelle, E.E., Marius, V., Julius, S., Alain, B., et al. (2017). Temperature monitoring in the vaccine cold chain in Cameroon. J. Vaccines. Vaccin. 09, 384–391. https://doi.org/10.4172/2157-7560.1000384.

Zapata, M.I., Feldkamp, J.R., Peck, G.E., White, J.L., and Hem, S.L. (1984). Mechanism of freeze-thaw instability of aluminum hydroxycarbonate and magnesium hydroxide gels. J. Pharm. Sci. 73, 3–8. https://doi.org/10.1002/jps.2600730103.

Zhang, B., Cao, H.J., Lin, H.M., Deng, S.G., and Wu, H. (2019). Insights into ice-growth inhibition by trehalose and alginate oligosaccharides in peeled pacific white shrimp (Litopenaeus vannamei) during frozen storage. Food Chem. 278, 482–490. https://doi.org/10.1016/j.foodchem.2018.11.087.

STAR★METHODS

KEY RESOURCE TABLE

REAGENT or RESOURCE	SOURCE	IDENTIFIER
Antibodies		
Goat pAb to Ms IgG1 (HRP)	Abcam	Cat: ab98693; RRID: AB_97240
Goat pAb to Ms IgG (HRP)	Abcam	Cat: ab97040; RRID: AB_205719
Chemicals, peptides, and recombinant proteins		
Alhydrogel®	InvivoGen	Cat: vac-alu-250 CAS: 21,645-51-2
EDA	XIYA REAGENT	Cat: 293,586 CAS: 107-15-3
Hepatitis B antigen	NCPC Genetech Biotechnology Co., LTD	N/A
n-Octyl-β-D-glucopyranoside	Sangon Biotech	Cat: A100479 CAS: 29,836-26-8
Trehalose	Sangon Biotech	Cat: A600966 CAS: 6138-23-4
Sucrose	Aladdin	Cat: C353425 CAS: 57-50-1
Aluminum nitrate nonahydrate	Kermel	CAS: 7784-27-2
PBS	Sangon Biotech	Cat: A610100
FBS	Thermo Scientific	Cat: 10,099
Critical commercial assays		
PierceTM BCA protein assay kit	Thermo Fisher Scientific	23,225
Micro BCATM protein assay kit	Thermo Fisher Scientific	23,235
The Cell Titer 96 AQueous One Solution Cell Proliferation (MTS) assay kit	Promega	G5421
RhinozymeTM Recombinant Factor C Endpoint Fluorescent Assay	Titan	2022–03
TMB	BD	555,214
Experimental models: Cell lines		
J774A.1 cells	ATCC	TIB-67™
Experimental models: Organisms/strains		
Mouse:C57BL/6	Liaoning Changsheng biotechnology co. Ltd.	N/A
Software and algorithms		
ImageJ	N/A	https://imagej.nih.gov/ij/
Jade 6.5	N/A	https://materialsdata.com/prodjd.html
Continued		
Other		
TEM, JEOL 1200 EX	JEOL	https://www.jeol.co.jp/
ORION STAR A214	Thermo Scientific	https://www.thermofisher.cn/cn/zh/home.html
D/Max 2400	Rigaku	https://www.rigaku.com/
90Plus Zeta	Brookhaven	https://www.bnl.gov/world/
1378	Thermo Scientific	https://www.thermofisher.cn/cn/zh/home.html
SpectraMax i3x	Molecular Devices	https://www.moleculardevices.com.cn/about-us
371	Thermo Scientific	https://www.thermofisher.cn/cn/zh/home.html
6700	Thermo Scientific	https://www.thermofisher.cn/cn/zh/home.html
TGA 4000	Perkin-Elmer	https://www.perkinelmer.com.cn/
ReadMax 1900	Shanghai Flash Spectrum Biotechnology Co., Ltd.	https://www.sangon.com/
LINKAM BCS196	LINKAM	https://www.astcorp.com.tw/makers/linkam
Olympus BX51	Olympus	http://cn.olympus.com/

RESOURCE AVAILABILITY

Lead contact

Further information and requests for resources should be directed to and will be fulfilled by the lead contact, Bingbing Sun (bingbingsun@dlut.edu.cn).

Materials availability

This study did not generate nor use any new or unique reagents.

Data and code availability

- All data reported in this paper will be shared by the lead contact upon request.
- This study did not generate any datasets.
- Any additional information required to reanalyze the data reported in this paper is available from the lead contact upon request.

METHOD DETAILS

Synthesis and freezing treatment of AlOOH nanorods

AlOOH nanorods were synthesized by using a hydrothermal method (Sun et al., 2013, 2017). To control the surface hydroxyl content, the AlOOH nanorods were prepared at 200°C for 2 or 6 h. Once the reaction was completed, the autoclave was immediately removed and cooled at RT. The precipitate was washed with deionized water for three times, and was dried for overnight at 60°C and stored at RT before use. For the freeze treatment, AlOOH nanorods were dispersed in water at 10 mg/mL and were stored at RT, −20°C and −80°C, respectively for 24 h. The frozen samples were then thawed at RT for 2 h. For the cryo-protect formulation study, adjuvant preparations containing 5% (w/v) trehalose, or 0.05% (w/v) octyl glucoside were stored at RT or −80°C. 24 h later, the formulations were thawed at RT for 2 h.

Physicochemical characterizations

Transmission electron microscopy (TEM, JEOL 1200 EX, JEOL, Japan) was used to determine the morphology of the AlOOH nanorods. X-ray powder diffraction (XRD, Rigaku D/Max 2400 type X-ray spectrometer) equipped with CuKα radiation (λ = 1.54178 Å) was used to determine the phase and crystallinity of the particles. All XRD patterns were collected with a step of 0.02° and counting time of 0.5 s per step over a 2θ range of 10–80°. A Zeta PALS instrument (90Plus Zeta, Brookhaven, USA) was used to determine the hydrodynamic sizes and the zeta potentials of the particles. The structural properties of AlOOH nanoparticles in suspensions were analyzed by Fourier transform infrared spectroscopy spectrometer (FTIR, 6700, Thermo Fisher, USA). Thermogravimetric analysis (TGA) was performed by heating the AlOOH NPs from RT to 800°C at a rate of 10°C/min under air in the air atmosphere using a Perkin-Elmer Diamond Thermogravimetric/Differential Thermal Analyzer (TGA 4000, USA). Potentiometric titration was performed to determine the amount of hydroxyl (Al-OH) groups on the particles surface (Meder et al., 2013). 50, 100 or 200 mg of nanoparticles were suspended in 35 mL of ultrapure water, and then were titrated with 0.05 M of KOH. The equivalence point (EP) was determined by using the maximum of the first derivative of the titration curve (d pH/d VKOH). The titration of deionized water (EPH$_2$O) was served as a control. To determine the suspension stability, AlOOH nanorods were dispersed in 0.9% NaCl aqueous solution at 1 mg/mL. The absorbance of the particle suspensions was measured at 232 nm (A232 nm) by a UV vis spectrometer (ReadMax, 1900, Shanghai Flash Spectrum Biotechnology Co., Ltd., China). Samples were monitored continuously for 12 h with an interval of 30 s. The absorbance of the particle suspensions at 0 h was considered as A0 232 nm, and the absorption intensity ratio, A232 nm/A0 232 nm, was taken as the degree of suspension stability, indicated by the suspension stability index (SSI). The recrystallization of ice in AlOOH NPs solution was determined using freezing stage (LINKAM BCS196, UK) (Chang et al., 2021; Wharton et al., 2007). Briefly, the ice sheets for observation were obtained by dropping solution from a height of 1.5 m onto the surface of the freezing stage. Then the nanoparticle solution was frozen to −80°C. The recrystallization was achieved by heating the frozen sample to −8°C within 5 min. The ice sheet was observed using a conventional microscope (Olympus BX51, Tokyo, Japan).

Adsorption of antigen

The assay buffer was prepared with 10 mM of MOPS and 50 mM of NaCl. The pH value was adjusted to 7.4 by diluted solution of hydrochloric acid or sodium hydroxide. For BSA adsorption, an equal amount of BSA working solution (1–5 mg/mL) and diluted adjuvant samples (1.7 mg/mL) that exposed to RT or −80°C were mixed in a microcentrifuge tube. For adsorption, the mixture was agitated at RT for 30 min, then centrifuged at 9000 rpm for 25 min. The supernatant was removed immediately and the protein concentration was determined using BCA assay kit. For HBsAg adsorption, adjuvant samples (0.27 mg/mL) that stored at RT or exposed to −80°C were mixed with HBsAg (50–250 μg/mL) at RT. The mixtures were incubated at RT for 30 min, and then centrifuged at 9000 rpm for 25 min. BCA assay was used to analyze the supernatant and determine the amount of HBsAg absorbed by the adjuvant samples.

Animal vaccination

Before the vaccination, the endotoxin level in AlOOH nanorods and octyl glucoside were determined using a Rhinogen Recombinant Factor C Endpoint Fluorescent Assay (Adamas life, Titan, Shanghai, China). Specific-pathogen free (SPF) female 6-week-old C57BL/6 mice were purchased from Sangon Biotech (Shanghai, China). All animals were raised under standard laboratory conditions in accordance with the guidelines approved by the Institutional Animal Care and Use Committee of Dalian University of Technology. In the vaccination studies, two experimental designs were included. In the first design, the adjuvants were exposed to −80°C, and then they were formulated with the antigen to prepare the vaccine. Mice (n = 6) were subcutaneously injected with HBsAg adsorbed freezing-treated or non-treated AlOOH nanorods (2 μg/50 μg) on day 0 and 21. As controls, mice were injected with saline buffer and HBsAg alone (2 μg) dissolved in saline buffer. In the second design, the vaccine was formulated (adjuvant + antigen) first, and then the whole vaccine formulation was exposed to −80°C. Mice were injected with freezing-treated or non-treated vaccines on day 0 and 21. As controls, mice were injected with saline buffer and HBsAg alone (2 μg) dissolved in saline buffer. On the 42th day after prime immunization, serum was collected to assess HBsAg-specific antibody responses. In brief, to analyze IgG_1 and total IgG, ELISA plates were first coated with 50 μg/mL HBsAg overnight at four°C, then blocked with PBS containing 10% FBS and exposed to serum samples. After that, biotin-conjugated goat anti-mouse IgG_1 or IgG antibody (10,000-fold dilution) were added into the plates, and the presence of bound antibody was detected in the presence of 3,3′,5,5′-tetramethylbenzidine solution (TMB, Sigma-Aldrich, USA). The absorbance was read at 450 nm (Liang et al., 2021).

Statistical analysis

For all the figures, the values shown represent mean $\pm$ SD Statistical significance was determined by two-tailed Student's t test for two-group analysis. Statistical significance was determined at $*p < 0.05$ and $**p < 0.01$.

ADDITIONAL RESOURCES

Any additional information in this paper is available from the lead contact on request.